e-cone and d-cone singularities drive submucosal collagen fiber remodeling in intestinal anastomotic surgery

Brian P. Fleischer[a.,1.], Nhung Nguyen[a.,1.], Anshuman Pal[b.,1.], Kameel Khabaz[a.], Alkiviadis Tsamis[c.], Efi Efrati[d.], Thomas Witten[b.], John C. Alverdy[a.], and Luka Pocivavsek[a.,2.]

[a.] Department of Surgery, The University of Chicago, Chicago, IL, USA; [b.] Department of Physics, The University of Chicago, Chicago, IL, USA; [c.] Department of Mechanical Engineering, University of Western Macedonia, Greece; [d.] Department of Physics of Complex Systems, Weizmann Institute of Science, Israel

Following resection of a diseased segment of intestine, reconnection (anastomosis) is configured with varying geometry (i.e. end-to-end, side-to-side, etc.). Yet proper healing of an intestinal anastomosis is not only a function of its geometry, but also its mechanobiology. We aimed to investigate the intersection of geometry, mechanical stress, and submucosal collagen fiber re-orientation as it pertains to a side-to-side small bowel anastomosis (SBA), the most common configuration performed in patients. Ten-week-old male C57BL/6 mice were assigned to creation of a side-to-side SBA or sham laparotomy. Anastomoses were analyzed at sacrifice on postoperative day (POD) 14 and 88 with histologic sectioning, staining, high-magnification imaging, and submucosal collagen fiber orientation (κ) mapping. The κ data, a measure of fiber dispersion, for sham-operated mice shows a mean and variance of 0.110798 and 0.00078 respectively, in close agreement with those values measured far away from the anastomosis (far-field locations) for mice sacrificed at POD 14. However, the mean and variance of κ at geometric-focusing locations for POD 14 become statistically significantly higher when compared to the sham population. At POD 88, the measurements of κ at all locations show no statistically significant difference and are comparable to the values measured for the sham group and the measurements at POD 14 for the far-field locations (p=0.096). Insight into the in vivo findings were further developed using a finite element model (FEM) of a simulated side-to-side anastomosis to model collagen reorientation. FEM demonstrated that anastomotic opening for the accommodation of flow generated high-stress areas within the afferent and efferent limbs. Our simulations predicted increased dispersion of submucosal collagen fibers, which may help to alleviate non-homeostatic mechanical stresses. The consistency across our FEM and experimental measurements reveals an underlying dynamic interaction between mechanical stress and collagen remodeling. By integrating various biologic, geometric, and computational approaches, a more complete understanding of the active nature of anastomotic construction can be advanced.

e-cone | d-cone | anastomosis |collagen fiber remodeling | stress focusing

Introduction

Surgery on the gastrointestinal (GI) tract generally involves removal (resection) of a diseased segment (cancer, inflammation) and its reconnection (i.e, an anastomosis) to reestablish continuity. The Achilles heel of this procedure involves unanticipated complications with healing such as tissues separation leading to leakage of toxic intestinal contents to over-healing with resultant strictures and occlusions of the new formed connection. In intestinal surgery, multiple anastomotic geometries are routinely performed including end-to-end, end-to-side and side-to-side, with side-to-side being the most common (Figure 1). These anastomoses can be configured in a peristaltic versus non-peristaltic manner. Despite the general clinical success of these procedures, the science and soft-tissue mechanics involved are only superficially understood. Different techniques for bowel anastomosis have been developed and debated (1) since the days of Halsted (2). The surgical canon is filed with discussions invoking geometry and mechanics, though largely from a phenomenological standpoint (1, 2, 8).

Surgeons can in large part manipulate the geometry of their anastomosis. The technical aspects of surgery are rooted in anatomy; anatomy is the spatial organization of tissue, i.e. geometry. Two fundamental phenomenologically-derived surgical principles are: maintain tissue integrity and strive for a 'tension-free' suture line (4, 5). The former confines any viable anastomotic geometry to a class of topology preserving shapes; meaning any combination of cutting and stitching is allowed however removal of tissue (beyond disease) is not. The latter imposes an even stronger condition on the suture line: length preservation or isometry. The field of intestinal surgery suffers from a fundamental lack of understanding of the geometry and mechanics underlying these principles. Advanced surgical devices such a staplers and robots have been engineered using empirical principles without a proper scientific basis. Commonly performed operations and hence complications (leaks, strictures, etc) still occur even when performed by expertly trained high volume surgeons operating in the most prestigious institutions. Therefore a most in-depth analysis of intestinal anastomotic construction is needed beyond those that have traditionally been ascribed to be causative to complications (ischemia, tension, technique) despite the lack of evidence.

The gastrointestinal track from a geometric standpoint is a long curvilinear cylindrical shell (9). Resection of an intestinal segment leaves the surgical problem of reestablishing continuity by forming an anastomosis, which amounts to bringing two

Significance Statement

B.F. and J.A. performed animal experiments; B.F., K.K., L.P. and A.T. performed collagen fiber orientation analysis; B.F., L.P., A.P. and N.N. performed finite element analysis; A.P., L.P., and T.W. performed geometric analysis; B.F., N.N., A.P., T.W., J.A., and L.P. wrote paper.

No conflicts of interest.

[1] B.F. , N.N , and A.P. contributed equally to this work.

[2] To whom correspondence should be addressed. E-mail: lpocivavsek@bsd.uchicago.edu

DRAFT

Fig. 1. Schematic of an end-to-end (left) and a side-to-side (right) intestinal anastomosis.

cylinders together following the above-mentioned established principals. Figure 3 outlines our geometric analysis of a general anastomosis. In physical shells, such as bowel, geometry impacts mechanics and in particular mechanical stability, which is intimately tied to the ability of thin shells to bend more easily than to stretch (10, 11). Over the last three decades, the rich field of thin sheet mechanics has unearthed how the balance of bending versus stretching often leads to solutions with strong geometric singularities and stress focusing (10, 11).

Prior work from our group explored the geometry of a simple transverse closure or the Heineke-Mikulicz strictureplasty, where the doubling of peri-anastomotic luminal bowel diameter is linked to the isometric deformation of the anti-mesenteric bowel wall (6). We showed that the strictureplasty shape, on the anti-mesenteric side, is determined by a geometric source point created at the middle of the suture line termed the excess or e-cone (7**?**). However, as shown in figure 3, the existence of e-cones is not limited to the strictureplasty. Indeed, such points ubiquitously appear as a consequence of imposing topology preservation. We show (figure 2) that the side-to-side anastomosis, which was largely created as a solution to the size-mismatch problems encountered in end-to-end anastomoses (figure 3), contains an e-cone. The impact of an e-cone embedded in a non-flat geometry remains an open problem. We show that an e-cone on a cylinder is always accompanied by a far-field singularity with non-zero Gaussian curvature which is also a source of stress focusing (figure 2). We prove that these far-field singularities are qualitatively and quantitatively crumpling-like structures akin to developable or d-cones (figures 4 and 5) (10**?** , 11).

In 1887, the great American surgeon Dr. William Halsted revolutionized gastrointestinal surgery through his discovery that the collagen-rich submucosa is the load-bearing layer of the intestinal wall (2). Previous work from our group has elucidated the critical role that submucosal collagen fibers play in anastomotic healing (13–15); breakdown of these fibers leads to anastomotic leak. In fiber-reinforced composites, fiber orientation plays a strong role in setting the global and local mechanics of the system (12, 25). Bowel is living matter endowed with the capacity to locally change tissue structure in response to stimuli. While many strong perturbations such as local injury, ischemia, and exposure to collagenolytic bacteria overwhelm the tissue's ability to respond and cause sub-mucosal collagen breakdown (13, 15), we hypothesize that "softer-modes" of collagen remodeling arise in peri-anastomotic regions with non-native stresses. In part two of this paper, we design the first ever clinically comparable end-to-end small bowel anastomosis mouse model and show that submucosal collagen remodels only in regions that correspond to the location of d-cones in our geometric and finite element analysis (see figure 6). Furthermore, we build a mechanical model that is able to predict the sub-mucosal biologic response. While such remodeling has been observed and studied in cardiovascular tissues (20), this is the first proof that it exists in gastrointestinal tissues and that remodeling is sensitive to the geometry of a surgical anastomosis.

The aims of the present study were to investigate the interaction between intestinal anastomotic geometry, mechanical stress, and collagen fiber distribution and remodeling. The approach was intended to be framed as a solution-agnostic thought experiment. We generate experimental data on submucosal collagen fiber distribution in surgically constructed anti-peristaltic side-to-side small bowel anastomoses in mice in conjunction with finite element modeling. Our central hypothesis is that the anti-peristaltic side-to-side anastomosis imposes a highly localized stress state on bowel tissue thereby altering its submucosal collagen structure through a remodeling process that is controlled by the tissue stress state imposed by its non-linear geometry. While other groups have attempted to recreate the anti-peristaltic side-to-side, functional end-to-end small bowel anastomosis in a murine model, our study is the first to do so in a physiologically relevant manner. Previous work from other groups(8), while aimed at creating a common channel congruous to that which we create in the operating room, falls short of what we are able to accomplish with our model. This allows us greater insight into the response of biologic tissue to the effects of non-linear anastomotic geometry.

Results and Discussion

Anastomotic Geometry. We simulate the bowel wall using two material laws: a single layer Ogden-Gasser-Holzapfel (OGH) model, with the material properties adopted from previous work on intestinal mechanics (12), or a homogenous hyperelastic Neo-Hookean model. Further details of material properties and boundary conditions are provided in the Methods section. Under applied luminal pressure, the anastomosis opens and FEM simulations show the existences of locations that exhibit geometric focusing and high stress. Figure 2 shows the representative deformed geometry of one limb under pressure and the common channel open to its maximum extent with diameter d_{max}. A side-to-side anastomosis when newly created is not spontaneously open, but remains in a closed configuration where $S_1 \parallel S_2 \parallel S_1^* \parallel S_2^*$. For a functional anastomosis, the intra-luminal pressure within the GI tract provides the needed force to open the anastomosis. Figure 2 outlines the basic geometric structure of a maximally open anastomosis using the deformed shape from our simulation. As the suture lines separate, they break the symmetry of the common channel into a portion which remains cylindrical, where $S_1 \parallel S_2$, and a portion that is conical. The geometric control parameter is ℓ, the distance between the two suture lines in their parallel configuration. Because a side-to-side anastomosis is functional only for a finite non-zero ℓ, it is key to understand its impact on the geometry. Focusing on a single limb, the bowel circumference, far from the anastomosis, is $C_0 = \pi d_0$; in the middle of the common channel, the

DRAFT

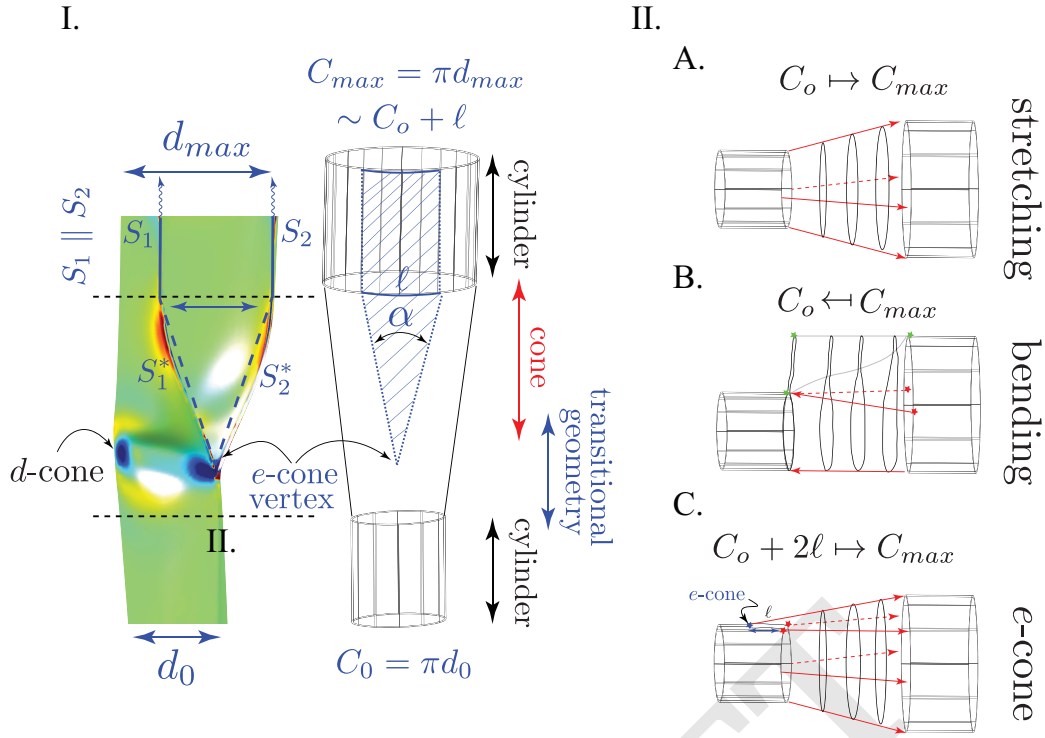

Fig. 2. The geometry of side-to-side and end-to-end anastomoses is dominated by mismatch in lengths of two cylinders. In the end-to-end anastomosis, **II.**, the mismatch is anatomic (physical) when the bowel is transected along a normal plane creating two circular cross-sections with circumferential lengths C_o and C_{max}. In the side-to side anastomosis, **I.**, the mismatch appears only when the anastomosis opens and is dynamic; here, C_{max} is a function of the anastomotic width ℓ which is a function of pressure. The Gaussian charge built up at the vertex is proportional to ℓ: $\alpha \sim 2\sin^{-1}\left(\frac{\ell}{2S_i^*}\right)$. Three topology preserving anastomotic geometries are possible in the end-to-end configuration. In **II.A.** the shorter suture line is mapped onto the longer one, mechanically this would lead to a tensile strain along C_o proportional to $\epsilon \sim C_{max}/C_o - 1$. Avoidance of tensile strains is a principle of gastrointestinal surgery; as such, **II.A.** is not representative of any surgical reconstruction. In **II.B.** the reverse mapping is performed, the longer suture line is brought to the shorter one. Two perfectly matched cylinders are created with C_o circumference in a tension free configuration; however, a region of excess material connected to the larger cylinder now appears (outlined between the three green stars). Mechanically this solution is dominated by compressive strains and therefor bending. It represents the canonical size-mismatched surgical reconstruction pioneered in the 19th-century by Theodor Billroth and dozens of subsequent variations throughout the 20th-century. **II.C.** is a topology preserving spatulated anastomosis, where the surgeon creates a cut of length ℓ along the longitudinal axis of the anti-mesenteric border such that $C_o + 2\ell \sim C_{max}$. Geometrically this is equivalent to one half of a transverse closure studied by our group (6, 7), with the appearance of an e-cone at the vertex of the enterotomy. The mechanical and biological consequence of e-cones on cylinders is central to this paper. The side-to-side anastomosis, **I.**, has a geometrical structure similar to **II.C.**: two length-mismatched cylinders connected via a transitional geometry dominated by an e-cone. Our focus is not on the e-cone itself, which we have investigated previously and which exists on the suture line, rather it is on the appearance of the non-isometric and stress focused region far-field from the suture line, labeled d-cone.

DRAFT

circumference of this same limb increases to $C_{max} \sim C_0 + \ell$, provided a cylindrical shape is maintained.

Figure 3 (top panel) shows the anastomosis with Gaussian curvature, K_g, calculated at each point on the surface. The majority of the surface has $K_g \sim 0$, meaning it is isometric to a plane, cylinder, or cone. There are two regions where $K_g \neq 0$; the first is along the suture line, where S_1 and S_2 transition from being parallel to approaching each other. A geometric interpretation of this transition is between a cylindrical region where S_i serve as the directors to a conical region where S_i^* become the new angled directors. Note that along the cone region of the common channel the non-zero Gaussian curvature is only along the suture line where it bends strongly. Eventually S_1^* and S_2^* meet at point, labeled e-cone vertex in figure 2. This marks the second region of non-zero K_g; in this transitional geometry, there is strong curvature focusing throughout and in particular the e-cone vertex where the suture lines meet and also far-field from it on the opposite bowel wall (mesenteric side). The side-to-side anastomosis is therefor geometrically the connection of two cylinders of different circumferences ($C_{max} >> C_0$) occurring through a transitional zone dominated by conical singularities.

As noted in the introduction, this problem is well known to surgeons. In figure 2 II., we outline the general problem encountered when attempting to connect two size-mismatched cylinders. There are only two solutions that preserve topology and require no additional cuts. One, $C_0 \mapsto C_{max}$, which causes stretching along C_0 and clinically is known to cause anastomotic failure due to tension. Two, $C_{max} \mapsto C_0$, which causes compression and therefor buckling along C_{max}; this is indeed the Billroth-I geometry, where one large buckle is created (a sort of internal circumferential 'dog ear') and sutured closed down to the vertex of the anastomosis creating the 'angle of Sorrow' (1); geometrically the shape of the 'dog ear' created on the large cylinder is a folded cone that connects smoothly to the remaining cylinder. If the excess length was more evenly distributed along the circumference a wrinkling pattern would appear. A third topology preserving solution exists, however it requires that a cut of length ℓ be made on the smaller cylinder such that $C_{max} \sim C_0 + 2\ell \equiv C_0^*$; $C_0^* \mapsto C_{max}$

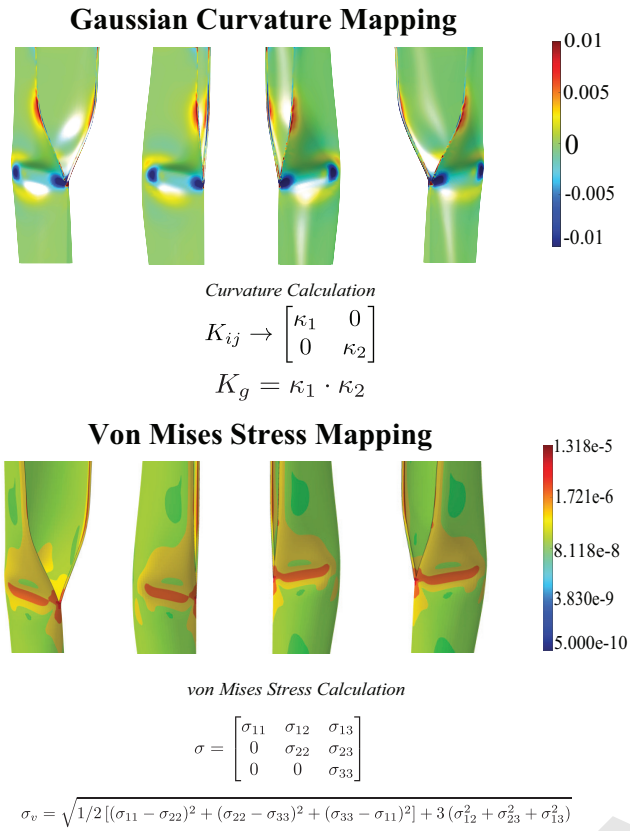

Fig. 3. Representative maximally deformed geometries of the open side-to-side anastomosis as simulated with finite elements. The principal curvatures are calculated at each point on the surface; Gaussian curvature, $K_g = \kappa_1 \cdot \kappa_2$, is mapped onto the surface showing that the majority of the deformed geometry is isometric to the undeformed cylinder, $K_g = 0$. Two regions of non-zero K_g exists: one on the suture line and two along a transitional region between the common channel and the limb (see figure 3 for geometric analysis). Bottom row shows the same deformed geometry with the stress field mapped onto the surface. Of note, the stress is nearly zero in all regions which deformed isometrically. However, the stress is three orders of magnitude above the baseline stress in regions corresponding to non-zero K_g; this indicates that the observed stress focusing is strongly linked to the underlying geometry.

is possible in a nearly tension free configuration, except at the cut vertex, which is an e-cone; this mapping, which one could call an 'anti-angle of Sorrow', is equivalent to one half of the strictureplasty closure we studied in the past (6, 7).

The transitional geometry encountered in the side-to-side anastomosis is similar to $C_0^* \mapsto C_{max}$ only softer. Before delving into the geometric and mechanical consequences of e-cones in cylinders, we point out that in certain configurations (such as two pieces of bowel of clearly different size) the geometric problem is easy to visualize; in others, such as the side-to-side anastomosis, it is less clear by simple inspection of the anastomosis, because the geometric incompatibility arises only through functional opening of the anastomosis. Alternatively, in the traditional end-to-end size-mismatched anastomosis, ℓ is static and constant; while in the side-to-side anastomosis, ℓ is a continuous function of pressure and ranges from zero in the initial configuration (most directly visible to the surgeon) to an upper bounda when the anastomosis if fully open.

While our prior work generated an e-cone on a cylinder, we did not systematically study its effect far-field form the e-cone vertex (6, 7). Bottom panel of figure 2 shows the stress distribution of the deformed shapes in the top panel; the transitional geometry shows a substantial increase in stress compared to the isometric cylindrical and conical regions. Comparing the top and bottom rows one can visually appreciate that non-zero K_g (geometric singularities) are linked to stress focusing.

The stress values shown are for a simulation performed using the OGH material model, which has biological relevance and is used later in this paper to study fiber remodeling. To more precisely study the stress distribution in this geometrically non-linear region, we performed simulations using a simpler Neo-Hooken material to be able to better compare with existing theories of conical singularities. Figure 4 shows the evolution of the stress pattern as a function of decreasing shell thickness; for the thickest shell, a singular center of high stress appears far-field from the e-cone and is connected by a ridge like region of higher than baseline stress. As the thickness decreases, the far-field structure bifurcates and generates a pattern reminiscent of those seen with the indentation of cylindrical shells (**? ?**); the observed patterns with indentation are similar to crumpling in flat sheets where high stress cores (called developable or d-cones) are connected by stretching or Witten ridges (11). While we do not study in detail the bifurcating pattern or its dependence on thickness, we do to prove that the cores are indeed d-cones. This analysis is lacking even in the indentation literature where the comparison to planar systems remains only qualitative.

DRAFT

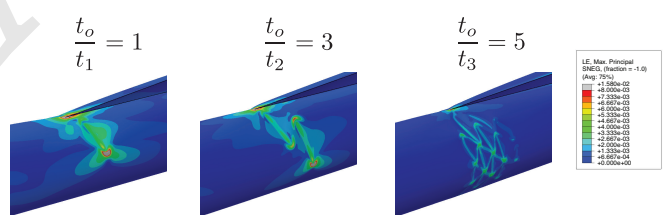

Fig. 4. Three side-to-side deformed geometries with anastomosis open generating a vertex e-cone in cylinders of varying thickness: $t_1/t_2 = 3$ and $t_1/t_3 = 5$ are shown. To quantitatively study the far-field mechanical and geometric consequences of the e-cone, we employ a simplified homogenous elastic material model in these simulations. In all three cases, all of the strain is again concentrated in the region of the transitional geometry as shown in figure 2, where the biologically relevant non-linear fiber-reinforced OGH material model is used. In all three cases, the e-cone vertex carries a large degree of tensile strain in a similar distribution. Interestingly, the far-field high-strain structures evolve in a cascading self-similar pattern with the thickest cylinder having a single crescent-like focus of high strain which bifurcates into two daughter centers which again bifurcate leading to a pattern qualitatively very reminiscent of crumpling. In crumpling, centers of high strain driven by non-isometric deformation called d-cones are connected by weaker strain-focused lines termed stretching ridges or the Witten ridge (11).

Figure 10 (appendix) shows our approach. Since there lacks a general theory of d-cones, we perform a comparison between the side-to-side geometry, where our hypothesis is that an e-cone drives the appearance of a remote d-cone, with a standard method of generating a simple d-cone in plane sheets, indentation of a sheet into a cylinder. Top panel in figure 10 shows the appearance of a simple d-cone as the elastic sheet evolves from a local stretching from indentation to global

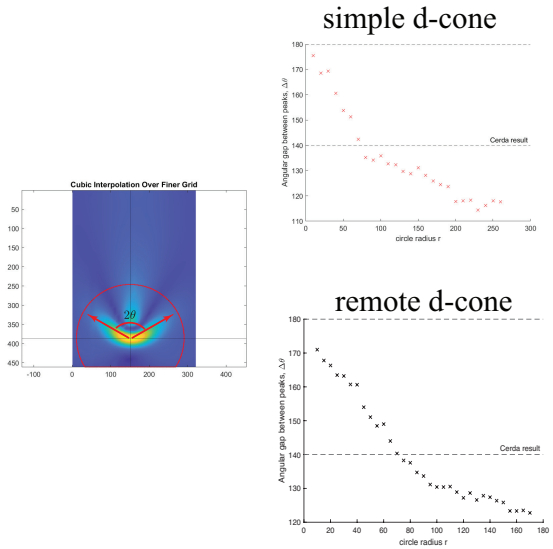

Fig. 5. The opening angle, 2θ, of the crescent-like strain distribution seen in d-cones is measured as a function of radial distance away from the peak core stress as outlined in figure 10. Note that the angle reaches an asymptotic limit once a given distance from the core itself. The simple d-cone shows a limiting $2\theta \sim 115^o$, while the remote d-cone has $2\theta \sim 125^o$. This proves quantitatively that the two structures are nearly identical and as such that the remote far-field strain focused singularity induced by the e-cone is a d-cone. Moreover, the opening angle falls into the theoretical range calculated for d-cones (**?**).

folding and local stress focusing as the d-cone evolves. Bottom panel in figure 10 shows the appearance and evolution of the remote high stress singularity in the side-to-side simulation. Given the boundary conditions and the loading there is no doubt that the planar indentation simulation is that of a d-cone. There is strong qualitative similarity between the appearance of the crescent-like strain distribution of the simple d-cone and the remote singularity in the cylinder. Figure 5 shows our data for the canonical d-cone opening angle 2θ plotted as a function of distance from the peak stress. The simplest theory of d-cones states that 2θ is constant at 140^0. (**?**), though this is only in the limit of linear elasticity and planar initial geometries. The nearly identical dependence of 2θ on radial distance for the two simulation, we believe, proves that the remote singularity being driven by the e-cone is indeed a d-cone.

Tissue Response to a d-cone.

Biological Experiments. Given the localization of Gaussian curvature and von Mises stress noted to occur remotely from the suture line (Figure 2), biologically-informed experiments were conducted to examine the distribution of the collagen fiber network in the submucosa of mouse small bowel at different time points in response to an anti-peristaltic side-to-side anastomosis. A side-to-side anastomosis was performed in ten week-old male C57BL/6 mice who, following recovery were sacrificed on either post-operative day (POD) 14 or 88. Anastomotic and peri-anastomotic tissues were harvested and sectioned at a pre-determined standardized depth to image both the isometric and the geometric focusing regions on the tissue as shown in Figure 2. The orientation of the submucosal collagen fibers was then imaged by staining the tissue with Trichome for histologic microscopy. We next measured and calculated

POD 14	POD 88
0.0482	0.1671
0.0119	0.2177
0.0722	0.288
0.0101	0.4499
0.0315	0.2197
0.0358	0.1494

Table 1. P-values demonstrating statistically significant difference between κ values of regions of isometric geometry and those experiencing geometric focusing.

the dispersion, κ, of the submucosal collagen fibers at different geometric locations and time points. This parameter, typically varying between 0 and 1/3, provides quantitative information on the state of fiber distribution. When $\kappa \rightarrow 0$, the collagen fibers are oriented in a completely aligned manner along a preferred mean direction. Alternatively when it approaches 1/3, the collagens are oriented in an isotropic (random, more dispersed) manner .

Results indicated that among κ values obtained from images taken at various locations, no stress-focusing was observed in our simulations nor in areas where we do see stress and curvature focusing in our simulations. Further, we found no statistically significant difference between these regions on POD 88. Conversely, with the exception of one sample, we did find a statistically significant difference between these regions on POD 14 (Table 1). These results were found regardless and independent of depth through the anastomosis in the z-direction. We observe that κ changes over time as we move spatially around the anastomosis. As shown in Figure 3, the portions of the anastomosis that experience regular stress fields and focusing have similar κ values regardless of post-operative time point. Conversely, we demonstrate a clear difference in the κ values calculated at the noted stress and curvature focused locations.

The distribution of κ for mice who have undergone a side-to-side anastomosis and subsequently sacrificed at POD 14 or 88 is demonstrated in Figure 2. Sham-operated mice (anesthesia, skin incision, and immediate closure) served as controls. The data for sham-operated mice shows a mean and variance of 0.110798 and 0.00078 respectively. This is in close agreement with the mean and variance of κ measured at isometric locations for those mice sacrificed at POD 14 (0.111635 and 0.0005807 respectively). Statistical comparison shows an insignificant difference between these two measurements (p=0.783). However, the mean and variance of κ at geometric focusing locations for POD 14 become statistically significantly higher when compared to the sham population (0.132298 and 0.0011772 respectively, p<0.0001). This suggests that the submucosal collagen fibers become more dispersed under the effect of geometric focusing. Interestingly, at POD 88, the measurements of κ at the isometric and geometric focusing locations show no statistically significant difference and are comparable to the values measured for the sham group and the measurements at POD 14 for the isometric locations (p=0.096).

While intestinal tissue is best modeled in its native state as a fiber-reinforced composite with two primary fiber-families running in a helical pattern through the submucosa in the theta-z plane(12), we observe a shift in the distribution of the orientation of submucosal collagen fibers in the immediate post-operative period. As noted in our POD 14 population,

DRAFT

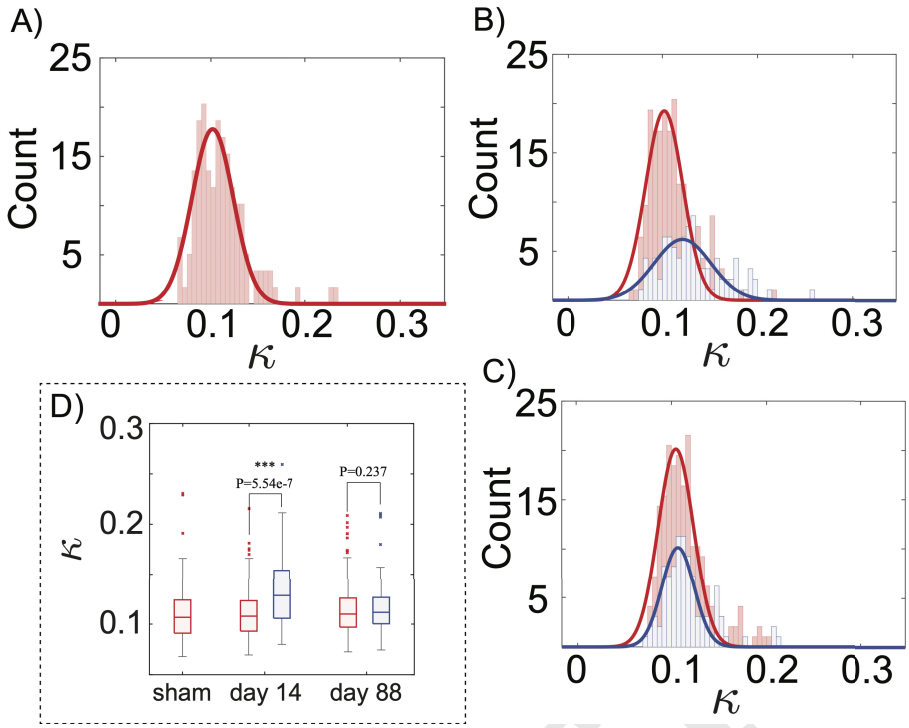

Fig. 6. Distribution of κ values through anastomosis as a function of location (red indicating regions of isometric geometry, blue indicating regions of geometric focusing) for A) Sham-operated mice as well as anastomoses harvested at B) POD 14 and C) POD 88. D) The regions of the anastomosis that experience isometric geometry have similar κ values regardless of post-operative time point, while there is a statistically significant difference at the noted geometric focusing location on POD 14 that reverts at POD 88.

there is a distinct and statistically significant difference in the orientation of the submucosal collage fibers when comparing those regions of bowel that experience standard stress fields with those that experience stress-focusing and d-cone deformation patterns, as informed by our simulations. This can likely be attributed to the biological tissue's desire to remodel in such a way so as to minimize the effects of these newly felt stress-focused fields. This shift in collagen fiber orientation leads the tissue away from its previous anisotropic response to stress to a more isotropic material, altering its deformation response to insults and likely its permanent function and appearance.

However, as post-operative time progresses, we note a return to the native orientation of these collagen fibers in those regions of the anastomosis that previously experienced stress-focusing and d-cone deformation patterns. This can likely be attributed to the permanent morphologic changes we observe in these anastomoses as they become grossly dilated and often fecalized at long time points. This adaptation of the affected bowel geometry via dilation leads to a relaxation in the stress-focusing initially felt after imposition of the non-linear geometry on the system, leading to re-organization of the submucosal collagen fibers into a conformation closely resembling its initial state. The scope of this work extends far beyond the bounds of this specific anastomotic construction. We know that similar geometric aspects that lead to the formation of stress-focused points exist in other commonly used conformations as well. The strictureplasty, an operation performed to relieve narrowing of the lumen of the bowel, results similarly in the formation of e-cones through its efforts to longitudinally open and transversely close an incision through the anti-mesenteric surface of the bowel(6).

Submucosal collagen fiber remodeling model. The next focus of this study is to explore the mechanism driving changes in the dispersion of submucosal collagen fibers in the above experiments. To elucidate this mechanism, we start the simulations with an aligned fiber state where the dispersion κ is set to zero and enrich the OGH model with a collagen fiber remodeling process induced by the stress focusing and loading state. The remodeling of the submucosal collagen fibers is triggered when the stress becomes larger than a critical value: $\sigma_{vs} > \sigma_{cr}$, here the Von-mises stress is used for an effective measure of stress state in FEM simulations of the anastomosis. This criterion in our model is motivated by active growth and remodeling phenomena in biological tissue which occurs when the homeostatic stress is perturbed (19). It also explains our experimental observation that changes in the dispersion of the collagen fibers were observed in the geometric, equivalently high stress areas, but not in the isometric ones. To explain the second observation in our experimental data that the collagen fibers in the geometric focusing regions become more dispersed, we hypothesized that the loading states played a role in governing this changes. This hypothesis is consistent with previous studies on collagen fibers remodeling (20). Specifically, collagen fibers tend to modify their orientations towards the principal loading directions. The two limiting cases are under simple uniaxial loading and equal biaxial loading. For the first limit, collagen fibers will remodel over time to align with the direction of the loading direction and hence reduce their dispersion $\kappa \to 0$. For the second limit, the tendency to orient towards principal loading directions leads to a more isotropic distribution of the collagen fibers and thus a more dispersed state is achieved where $\kappa \to 1/3$ (20). These tendencies have been incorporated to study collagen remodeling in aortic valve, which exhibit

a more complex loading situation (20). However, they have not been applied to study the remodeling induced by the side-to-side anastomosis construction and with the complex and non-linear fiber-reinforced feature of the OGH model. Therefore, we developed a second criterion that is able to incorporate the tendency of collagen fibers to remodel towards principal loading directions with OGH model. The developed model is able to explain how the submucosal collagen fibers re-orient as the anastomosis is pressurized.

Specifically, for the elements that experience a stress that is above the threshold value σ_{cr}, the stretches λ_1, λ_2 along the principal circumferential and longitudinal directions are determined. These values provide the loading states that dictate the preferable dispersion value κ_p of the collagen fibers. Denote $g_i = \lambda_i - 1$, where $i = \overline{1,2}$. If $|g_1| * |g_2| > 0$, the element exhibits a biaxial stress state and therefore the preferable direction of the collagen fibers are determined as follows:
For $|g_1| > |g_2|$:

$$\kappa_p = \frac{1}{3}\frac{|g_2|}{|g_1|} \qquad [1]$$

For $|g_2| > |g_1|$:

$$\kappa_p = \frac{1}{3}\frac{|g_1|}{|g_2|} \qquad [2]$$

Note that if $|g_1| \gg |g_2|$, the element experiences a near uniaxial loading state. Hence, from Equation 4, the preferable value of κ_p becomes 0 as in the limit of uniaxial loading. In other words, the collagen fibers remodel toward the principal uniaxial loading direction, and thus exhibits a more aligned state. The same limit is obtained from Equation 5 if $|g_2| \gg |g_1|$. On the other hand, if $|g_1| = |g_2|$ then both Equation 4 and 5 gives the limit of an equal biaxial loading in which κ_p becomes 1/3. This means that collagen fibers becomes more dispersed and experience a more isotropic distribution. For any state of loading in between the preferable value of the dispersion can be obtained from Equations 4 and 5. Since we start with the assumption of $\kappa = 0$, the condition $|g_1| * |g_2| < 0$ that resembles a uniaxial loading state does not cause a change in the dispersion value: $\kappa_p = \kappa = 0$. However, future development of the computational model can include an improvement for this assumption where a more non-homogeneous initial dispersion state is assumed.

The remodeling happens to adjust the initial fiber dispersion of each element towards the targeted preferable direction dictated by the loading state as established above. A remodeling rate equation (20) is used to govern this adjustment process:

$$\frac{d\kappa}{dt} = \frac{1}{\tau}(\kappa_p - \kappa) \qquad [3]$$

where τ is the rate of the remodeling.

The above model is implemented using the user material subroutine VUMAT in Abaqus. Details of the subroutine implementation are provided in the Appendix. Our simulations are able to couple the non-linear, complex loading situations of a pressurized side-to-side anastomosis with the evolution of the dispersion value updated based on the remodeling Equations 4-6. The rate of the remodeling is adjusted by varying τ, hence provides a capability to capture how fast or slow the remodeling happens in real experiments. Simulations with our developed model shows that the anastomosis opens and in the stress focusing regions the stress states are close to an equal biaxial stress state that drives the submucosal collagen fibers to experience a more dispersed state: $\kappa_p \to 1/3$. Figure 2 shows this increase of the κ value from the initial dispersion state. The distribution of the dispersion values from the numerical simulations at the end of the remodeling process is qualitatively consistent with the experimental measurement shown in Figure.

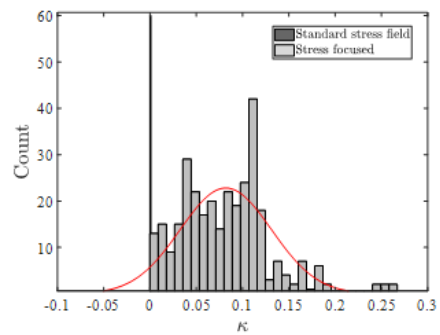

Fig. 7. FEM simulations with a collagen remodeling fiber shows the increase of dispersion value in the stress focused region.

Conclusions

Since collagen fibers have been reported to have the capacity to remodel under applied stress (20), we investigated how stress is distributed along the amorphous non-linear configuration of a side-to-side anastomosis and its association with changes in collagen fibers. We developed both a novel operative technique to create a physiologically relevant small bowel side-to-side anastomosis as well as a new stress induced remodeling model coupled with OGH constitutive modeling incorporating criteria from previous experimental and numerical studies on collagen remodeling (20). Firstly, remodeling only occurs if the applied stress is greater than a set critical value. This finding is consistent with our experimental data where the changes in fiber dispersion are only observed in stress-focusing areas. Secondly, collagen fibers remodel in a manner in which the dispersion value depends on the loading states with two limits. If the loading state is equal biaxial, the collagen becomes more dispersed and it becomes more aligned in the uniaxial loading state. Due to the first criterion, the collagen fibers only remodel in the stress focus regions, which is again demonstrated in our biological experiments. This explains why there are no changes in collagen dispersion in the non-stress-focused regions in our experimental data. The second criterion further predicts that the dispersion becomes higher, indicating a more dispersed fiber state in these areas. Furthermore, our model predicts that after remodeling occurs, the stress of the elements inside the remodeling area drop, alleviating the stress focusing effect that the bowel experiences.

Materials and Methods

***In Vivo* Model.** All mouse experiments were approved by the Institutional Animal Care and Use Committee (IACUC) of the University of Chicago (ACUP protocol 72417). Ten week-old male C57BL/6 mice (Charles River Laboratories©, Kingston,

DRAFT

NY) were used for all experiments and were allowed unrestricted access to standard chow diet and tap water both pre- and post-operatively. All mouse experiments were run in duplicate.

All non-control or sham-operated mice were anesthetized and underwent laparotomy with handsewn small bowel anti-peristaltic side-to-side, functional end-to-end anastomosis using 8-0 monofilament, non-absorbable suture (Surgipro^{TM} II Monofilament Polypropylene), following appropriate sterile technique. Laparotomy incision was closed in two layers using 3-0 braided, absorbable suture (Covidien Polysorb^{TM}). Anesthesia was obtained via intra-peritoneal injection of 100 mg/kg ketamine and 10 mg/kg xylazine(21). Post-operatively, all mice were resuscitated with 1mL sterile water injected subcutaneously. Intra-operatively, a segment of small bowel was identified and transected, with special attention paid to ensure there was no interruption of blood supply to the bowel. The two ends of the bowel were spatulated along the anti-mesenteric surface and the common channel of the anti-peristaltic side-to-side, functional end-to-end anastomosis was created. The common anastomotic channel length was approximately 2-3 times the diameter of the bowel lumen.

A. Tissue Harvesting and Histology. The mice were sacrificed on either POD 14 or 88. The previous laparotomy incision was re-opened and the underlying bowel was carefully dissected out. The anastomosis and peri-anastomotic tissues were harvested and pressurized with 100μL of formalin to ensure bowel was fixed in a non-collapsed conformation. All harvested tissue was then formalin fixed and embedded in paraffin to prepare for sectioning and staining.

Tissue samples were sliced into 5μm thick sections, which subsequently underwent Trichome staining. Sections were obtained at pre-determined depths, correlating with entry into the lumen of the bowel and areas of predicted stress-focusing as calculated using our computer simulations.

B. Sample Imaging. All sample imaging was performed at 100x/1.3NA oil 0.2mm WD magnification using a Zeiss Axioskop^{TM} upright histology microscope. Images were captured around the perimeter of each sample at predetermined locations, approximately every 0.2mm of tissue.

C. Image Analysis. Initial image analysis was performed through Fiji and its Directionality plugin (v2.0). All captured microscopy images were cropped such that only the submucosal collagen fibers were included and rotated such that the horizon was set to 0°. The aforementioned program was then implemented to characterize the orientation of submucosal collagen fibers in each image via a Fourier Transformation. These results were confirmed using a separately validated image processing algorithm(22).

D. Data Analysis. The collagen fibers of the small intestinal submucosa were assumed to consist of an interweaving lattice structure of two distinct fiber populations that run along the longitudinal axis of the bowel and intersect in a cross-ply fashion(12, 23). Further, it was assumed that the collagen fibers are distributed according to a transversely isotropic and π-periodic von Mises distribution, which is commonly assumed for directional data. We normalized the standard π-periodic von Mises distribution with the resulting distribution in Equation 7(24).

$$\rho(\theta) = 4\sqrt{\frac{b}{2\pi}}\frac{exp[b(cos(2\theta)+1)]}{erfi(\sqrt{2b})} \qquad [4]$$

Our raw data obtained via image analysis techniques previously described were plotted and fit to the above curve. After solving for the concentration parameter b in Equation 1, we solved for the structural parameter κ using Equation 8(25).

$$\kappa = \frac{1}{2} + \frac{1}{8b} - \frac{1}{4}\sqrt{\frac{2}{\pi b}}\frac{exp(2b)}{erfi(\sqrt{2b})} \qquad [5]$$

E. Statistical Analysis. Images obtained around the perimeter of each sample at predetermined locations were siloed into locations where we do not see stress-focusing in our simulations and those areas where we see geometric and stress focusing in our simulations. The κ values previously obtained for every image captured were then compared between these two silos using a one-tailed, two-sample unpaired t-test for samples of unequal variance.

F. Finite Element Modeling. A computational model for a side-to-side anastomosis was constructed in the commercial finite element (FE) software Abaqus (Dassault Systemes, RI) (16) as shown in Supplemental figure 1. Specifically, a slit was created on the wall of a cylinder to model the suture lines on the anti-mesenteric surface of the tubular bowel. In the finite element simulations, we model only one limb of the anastomosis, assuming symmetry with the second. This is done to decrease the computational cost of the simulation, since simulations with both limbs showed no appreciable differences compared to the single limb simulation (see supplemental video 1 and supplemental video 2). Boundary conditions along the suture line are used to reproduce the mechanical effect of the kinematic coupling that the sutures impose. Pressure due to the flow of the luminal contents inside the bowel was applied to the internal surface to drive the opening of the anastomosis. The main load bearing layer of the intestinal wall, the submucosa, is a fiber-reinforced layer with collagen distributed in the soft elastin matrix (12, 17, 18). To capture this structural aspect and the large deformation of the bowel tissue, the Ogden-Gasser-Holzapfel (OGH) model was utilized (12, 17, 18). We simulate the bowel wall as a single layer OGH model with the material properties adopted from previous work on intestinal mechanics (12): $\mu = 1.58$ kPa, $k_1 = 22.01$ kPa, $k_2 = 12.1$, and $\kappa = 0$. The mean collagen fiber direction in the submucosa layer is $\theta = 30^0$ as suggested in (12). The model is based on a strain-energy function $\Phi = \Phi_m + \Phi_f$ composed of contributions from the elastin matrix Φ_m and the collagen fibers Φ_{fi}. The specific forms for these energy functions are as follows:

$$\Phi_m = \frac{\mu}{2}\left(\bar{I}_1 - 3\right) + \frac{K}{2}\left(\frac{J^2-1}{2} - ln(J)\right) \qquad [6]$$

$$\Phi_{fi} = \frac{k_1}{2k_2}\left[\exp\left(k_2\bar{E}_i^2\right) - 1\right] \qquad [7]$$

$$\bar{E}_i = \kappa\left(\bar{I}_1 - 3\right) + (1-3\kappa)\left(\bar{I}_{4i} - 1\right) \qquad [8]$$

where μ and K are the shear and bulk modulus of the elastin matrix, respectively, $J = det(F)$ represents the volume ratio between the deformed and undeformed tissue with F is the

DRAFT

deformation gradient. To enforce a nearly incompressible behavior for the bowel material (12) where $J \to 1$, a high numerical value for the ratio K/μ was used. $\bar{I}_1 = J^{-2/3} I_1$ where $I_1 = tr(C)$ is the first invariant of the right Cauchy Green tensor $C = F^T F$ widely used to study the nonlinear elasticity of soft elastomeric materials and tissues (12, 17, 18). Two symmetric families of collagen fibers $i = 1, 2$ are assumed to orient along an angle $\pm\theta$ with respect to the circumferential direction, corresponding to two mean directions A^i (12). k_1 is the fiber stiffness, and k_2 is a dimensionless parameter correlating to the non-linearity of the collagen fiber's response. κ is the dispersion of the collagen fibers. $\kappa = 0$ corresponds to an aligned state of collagen fibers along the mean direction and $\kappa = 1/3$ corresponds to an isotropic dispersion state. $\bar{I}_{4i} = J^{-2/3} I_{4i}$ and $I_{4i} = A^i.CA^i$ gives the square of the stretch along the mean direction A^i of the ith fiber family.

G. d-cone analysis. *Need Neo-Hookean parameters for the Geometry simulations.*

Our analysis is done at a fixed time step, far along into the simulation that we can safely assume a steady-state stress distribution has been attained. We import the (von Mises) stress data for the region of interest (i.e., the region around the cut tip) from Abaqus to Matlab using the package Abaqus2Matlab (**?**). This data is defined on the undeformed cylinder. For ease of viewing and subsequent analysis, we unroll and flatten the cylinder to a rectangle, using the standard mapping $(\theta, z) \mapsto (x, y)$, where θ is the azimuthal coordinate and z is the axial coordinate on the cylinder. Finally, using peak detection, we isolate the point singularity we wish to study, and keeping in mind the measurements to follow, also interpolate this isolated data over a fine grid (see supplemental figure 2A). We wish to measure quantities along the arc of the crescent singularity, i.e., as a function of the arc length coordinate s. In other words, we wish to extract a meaningful 1-dimensional data field, say $\sigma(s)$ for stress, from a 2-dimensional one, $\sigma(x, y)$. To do this, we draw circles of increasing radius r centered at the tip of the crescent (located using peak detection algorithms), and measure σ only along this circular contour. Here, the radius $r \approx s$, the desired arc length coordinate, since the crescent is not sharply curved. This gives a polar distribution of the data along the circle (as a function of the angle ϕ), which has a tri-lobular structure, as expected (each lobe is a maximum or peak), see supplemental figure 2B. Since we are only interested in the crescent here, we only care about the two side peaks. Again, using peak detection, we find the angular locations of the three lobes. Shifting the central peak to the y-axis ($\phi = 0$), we can then measure the opening angle of the two side lobes, call them ϕ_1 and ϕ_2. Measurements show that $\phi_1 = -\phi_2 = \phi_{cresc}$. This gives us a value for that particular circle, of radius r. Doing this for a range of circles, we get the desired distribution $\phi_{cresc}(r) \approx \phi_{cresc}(s)$ along the arc of the crescent. The d-cone opening angle is $\Delta\theta = 2\phi_{cresc}$. Similarly, we can get the stress along the two arms of the crescent, $\sigma_1(s)$ and $\sigma_2(s)$. Measurements also show that $\sigma_1(s) \approx \sigma_2(s)$. The same analysis applies to the simple d-cone situation, with the just the initial data preparation being simpler since the undeformed geometry is already a rectangle, and not a cylinder.

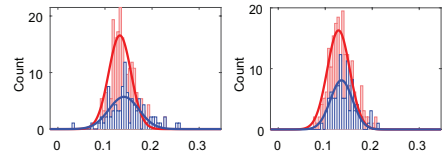

Fig. 8. Confirmatory tests performed with a separately validated algorithm demonstrate results in good agreement with those derived with our method of data acquisition and analysis.

Appendix

ACKNOWLEDGMENTS. Please include your acknowledgments here, set in a single paragraph. Please do not include any acknowledgments in the Supporting Information, or anywhere else in the manuscript.

1. Aly OE. A new direction in anastomotic research: should we redesign the 'angle of sorrow'? *Int J Colorectal Dis*, 33(2):159–162, 2018.
2. Halsted WS. Circular suture of the intestine – an experimental study. *Am J Med Sci*, 188: 436–461, 1887.
3. Jordan Ellenberg. *Shape: The Hidden Geometry of Information, Biology, Strategy, Democracy, and Everything Else*. Penguin Press, 2021.
4. Yeo CJ, Matthews JB, and McFadden DW et al. *Shackelford's Surgery of the Alimentary Tract*. Saunders, 2012.
5. Hawley PR. Causes and prevention of colonic anastomotic breakdown. *Dis Colon Rectum*, 16 (4):272–277, 1973.
6. Pocivavsek L, Efrati E, and Lee KYC et al. Three-dimensional geometry of the heineke–mikulicz strictureplasty. *Inflamm Bowel Dis*, 19:704–711, 2013.
7. Tsamis A, Pocivavsek L, and Vorp DA. Elasticity and geometry: a computational model of the heineke–mikulicz strictureplasty. *Biomech Model Mechanobiol*, 13(6):1185–1198, 2014.
8. Gajendran M, Bauer AJ, and Buchholz BM et al. Ileocecal anastomosis type significantly influences long-term functional status, quality of life, and healthcare utilization in postoperative crohn's disease patients independent of inflammation recurrence. *Am J Gastroenterol*, 113(4): 576–583, 2018.
9. Savin T, Kurpios NA, and Shyer AE et al. On the growth and form of the gut. *Nature*, 476: 57–62, 2011.
10. Audoly B and Pomeau Y. *Elasticity and Geometry: From hair curls to the nonlinear response of shells*. Oxford University Press, 2010.
11. Witten TA. Stress focusing in elastic sheets. *Rev Mod Phys*, 79:643–675, 2007.
12. P Ciarletta, P Dario, F Tendic, and S Micera. Hyperelastic model of anisotropic fiber reinforcemens within intestinal walls for applications in medical robotics. *Int J Robotics Research*, 28 (10):1279–1288, 2009.
13. Hyoju SK, Klabbers RE, and Aaron M et al. Oral polyphosphate suppresses bacterial collagenase production and prevents anastomotic leak due to serratia marcescens and pseudomonas aeruginosa. *Ann Surg*, 267(6):1112–1118, 2018.
14. Shogan BD, Belogortseva N, and Luong PM et al. Collagen degradation and mmp9 activation by enterococcus faecalis contribute to intestinal anastomotic leak. *Sci Transl Med*, 7(286): 286ra68, 2015.
15. Shakhsheer BA, Versten LA, and Luo JN et al. Morphine promotes colonization of anastomotic tissues with collagenase - producing enterococcus faecalis and causes leak. *J Gastrointest Surg*, 20:1744–1751, 2016.
16. Abaqus. *Abaqus User's Manual, Vs.6.18*. Dassault Systemes, Simulia Corporation,RI, 2018.
17. T C Gasser, R W Ogden, and G A Holzapfel. Hyperelastic modelling of arterial layers with distributed collagen fiber orientations. *J R Soc Interface*, 3(6):15–35, 2006.
18. N Nguyen, N Nath, L Deseri, E Tzeng, S S Velankar, and L Pocivavsek. Wrinkling instabilities for biologically relevant fiber-reinforced composite materials with a case study of neo-hookean/ogden–gasser–holzapfel bilayer. *Biomech Model Mechanobiol*, 19:2375–2395, 2020.
19. P Saez, E Pena, M A Martinez, and E Kuhl. Computational modeling of hypertensive growth in the human carotid artery. *Comput Mech*, 53:1183–1196, 2014.
20. N J B Driessen, M A J Cox, C V C Bouten, and F P T Baaijens. Remodelling of the angular collagen fiber distribution in cardiovascular tissues. *Biomech Model Mechanobiol*, 7(2):93–103, 2008.
21. Ward MA, Pierre JF, and Leal RF et al. Insights into the pathogenesis of ulcerative colitis from a murine model of stasis-induced dysbiosis, colonic metaplasia, and genetic susceptibility. *Am J Physiol Gastrointest Liver Physiol*, 310:G973–G988, 2016.
22. Koch RG, Tsamis A, and D'Amore A et al. A custom image-based analysis tool for quantifying

DRAFT

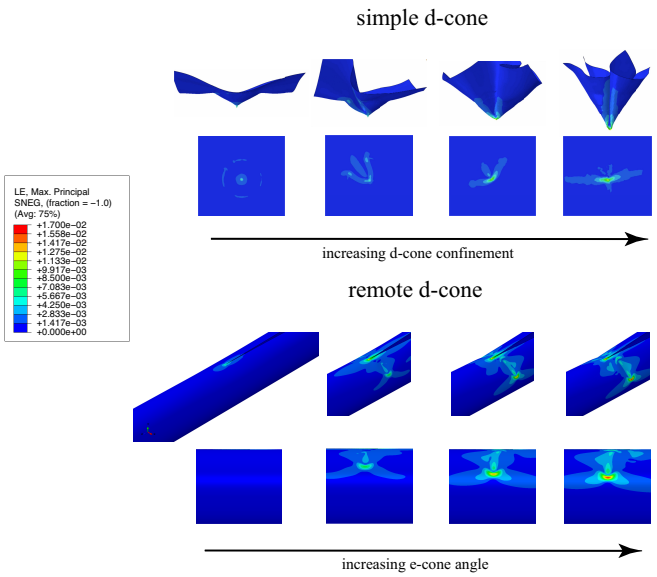

Fig. 9. The evolution of the far-field strain pattern with thickness (figure 4) qualitatively supports the hypothesis that this region of the cylinder deforms by forming d-cones locally. Given the lack of a general theory of d-cones, to prove that the remote singularity seen in our simulations is indeed a d-cone, we opted to compare the strain distribution of a simulated simple d-cone with the remote far-field d-cone. The simple d-cone is generated by indenting a flat membrane into a hollow cylindrical support, this is the classic loading geometry well known to generate a d-cone at the point of indentation (11?). We show both the deformed geometry and the projected strain distribution onto the undeformed initial shape. For the simple d-cone, the initial core region shows a symmetric strain distribution as expected for localized stretching due to indentation. Once the membrane undergoes a macroscopic bending/folding, the classic crescent-like distribution of strain at the d-cone core appears (?). With further confinement, the crescent distribution remains focused but evolves in its shape for an elastic systems such as simulated here. The bottom row shows the evolution of a single remote d-cone on the cylinder with increasing e-cone angle; the same crescent shape is observed in the strain distribution around the core. This data shows that the simple d-cone and the remote d-cone have qualitatively the same distribution of strain in the core region, allowing us to make the claim that the far-field high strain singularity in the cylinder is indeed a d-cone.

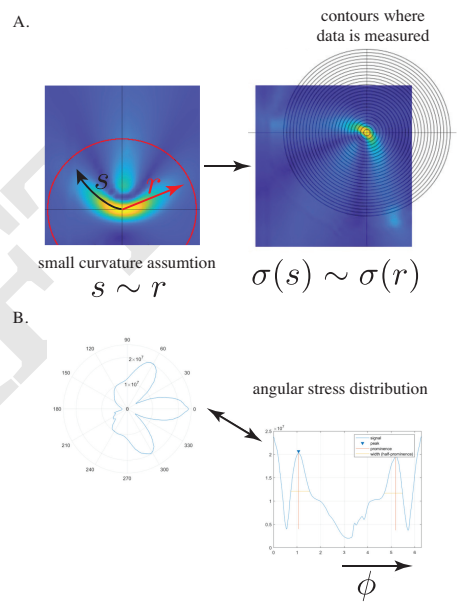

Fig. 10. To allow for a quantitative comparison of the different d-cone structures beyond the qualitative comparison provided in figure 9, we measure the evolution of the stress as a function of distance from the peak stress. As explained in the methods, this is done by generating concentric contours on the flattened surfaces, and working in the small curvature limit $s \sim r$, generating a map of $\sigma(r)$ data. This allows us to measure the opening angle of the d-cone as a function of distance (data shown in figure 5).

elastin and collagen micro-architecture in the wall of the human aorta from multi-photon microscopy. *J Biomech*, 47(5):935–943, 2014.

23. Zeng YJ, Qiao AK, and Yu JD et al. Collagen fiber angle in the submucosa of small intestine and its application in gastroenterology. *World J. Gastroenterol*, 9(4):804–807, 2003.
24. Annaidh AN, Bruyere K, and Destrade M et al. Characterization of the anisotropic mechanical properties of excised human skin. *J Mech Behav Biomed Mater*, 5(1):139–148, 2012.
25. Ogden RW. *Nonlinear Continuum Mechanics and Modeling the Elasticity of Soft Biological Tissues with a Focus on Artery Walls. In: Holzapfel G., Ogden R. (eds) Biomechanics: Trends in Modeling and Simulation. Studies in Mechanobiology, Tissue Engineering and Biomaterials*, volume 20. Springer, 2017.

DRAFT